IMPROVED VESSEL DEPICTION OF THE CAROTID ARTERIES AND BIFURCATION WITH A SPECIALIZED 16-CHANNEL PHASED ARRAY COIL

by

Quinn Tate

A thesis submitted to the faculty of
The University of Utah
in partial fulfillment of the requirements for the degree of

Master of Science

Department of Electrical and Computer Engineering

The University of Utah

August 2011

Copyright © Quinn Tate 2011

All Rights Reserved

The University of Utah Graduate School

STATEMENT OF THESIS APPROVAL

The thesis of **Quinn Tate**

has been approved by the following supervisory committee members:

Cynthia Furse	, Chair	**April 22, 2011** Date Approved
Om Gandhi	, Member	**April 22, 2011** Date Approved
Dennis Parker	, Member	**April 22, 2011** Date Approved

and by **Gianluca Lazzi** , Chair of

the Department of **Electrical and Computer Engineering**

and by Charles A. Wight, Dean of The Graduate School.

ABSTRACT

Magnetic resonance imaging (MRI) is a robust imaging modality that can utilize specialized receive only coils (antennas designed to be sensitive in the near field). The purpose of this thesis is to design and construct a multichannel receive-only RF coil for 3 Tesla magnetic resonance imaging of the human carotid artery and bifurcation with optimized signal to noise ratio (SNR) in the carotid vessels along the full extent of the neck. A neck phantom designed to match the anatomy of a subject with a thick short neck, representing a body habitus often seen in subjects with carotid arterial disease, was constructed. Sixteen circular coil elements were arranged on a semi-rigid fiberglass former that closely fit the shape of the phantom, resulting in a 16-channel bilateral phased array coil. Comparisons made between this coil and a four-channel carotid coil in a study of 10 carotid vessels in 5 healthy volunteers showed a 70% average improvement in signal to noise ratio (SNR) at the bifurcation with the 16-channel carotid coil. This coil also maintains an SNR greater than the peak SNR of the four-channel coil over a vessel length of 10 cm. This increase in SNR results in improved vessel depiction of the carotid arteries over an extended field of view, and demonstrates better image quality for higher parallel imaging reduction factors compared to the four-channel coil.

TABLE OF CONTENTS

ABSTRACT ……..... iii

LIST OF FIGURES ……...…….. v

CHAPTERS

1. INTRODUCTION 1

1.1 Improved MRI of carotid bifurcation..... 1

2. BACKGROUND 5

2.1 Magnetic field 5
2.2 Producing a signal 6
2.3 Acquiring the signal 12
2.4 Processing the signal 13

3. COIL DEVELOPEMENT 15

3.1 Current four-channel standard..... 15
3.2 Six and eight channel carotid coils..... 16
3.3 Improvements to existing designs 17

4. JOURNAL PAPER..... 21

4.1 Increased Vessel Depiction of the Carotid Bifurcation with a Specialized 16-Channel Phased Array Coil at 3T..... 22

5. SUMMARY, CONCLUSIONS AND FUTURE WORK..... 38

5.1 Summary 38
5.2 Conclusions 39
5.3 Future work 40

REFERENCES …….. 41

LIST OF FIGURES

Figure

1.1: New 16 channel coil……... 4

2.1: Magnetization vectors…..…… 8

2.2: A simple example of an MRI timing diagram……... 10

3.1: Overlapping of rectangular loops with a compensating overlap…….....18

CHAPTER 1

INTRODUCTION

1.1 Improved MRI of carotid bifurcation

One of the leading causes of death in the United States is stroke, and one of the leading causes of stroke is arterial disease. Arterial disease in the carotid artery in most cases can be detected first in the carotid bifurcation. While there are many different imaging modalities, magnetic resonance imaging (MRI) has the ability to provide the best resolution of soft tissue noninvasively and hence best resolution of the carotid bifurcation. This imaging is hampered by the small size of the plaque morphology, the variable position and depth of the artery in many subjects, variations in external body habitus, and the tendency for subjects to move or swallow during imaging. These four limitations form the basis of this research to build a custom MRI receive only coil, designed specifically for imaging the carotid bifurcation. This research will address these concerns by increasing the signal to noise ratio (SNR) over a larger region, creating a closer fitting neck former and by effectively reducing scan time.

The received signal intensity, and consequently SNR, of an MR image is partially dependent upon the strength of the static magnetic field used to acquire images. Therefore, one approach to increasing SNR is to increase the strength of the magnetic field. This is an expensive option and because of FDA safety restrictions, is

not available to everyone. SNR is also highly dependent upon the sensitivity of the antenna arrays used to receive the signal. These antenna arrays are designed to receive signal in the near field and due to their distinct function, they are referred to as coils and not antennas. There are several different types of MRI coils. Volume and surface coils are the most common. It is possible to use a coil as a transmitter as well as a receiver. In general this work will refer to an MRI receive-only surface coil as simply a coil.

Currently, the standard four-channel coil design includes a two-channel nuclear magnetic resonance (NMR) phased array (PA) on each side of the neck designed to image at a depth of 3 to 5 cm. The design of this PA provides a much higher SNR than a single coil [1]. The received noise decreases by reducing the sensitive volume of the RF coil and the signal will increase by placing the coil close to the measurement area. However, this four-channel design is limited in its coverage, signal acquisition and in fitting the contours of individual patient anatomy. These difficulties limit imaging with this coil to only a small portion of the body. Also, time needed to scan or image a patient is always an important consideration both on behalf of the patient and the physician. Lengthy scan times lead to an uncomfortable patient, which can add to patient motion, resulting in lower image quality.

My research will determine the improvement in coverage and SNR that is possible with an alternative, ergonomic coil design. This alternative design has been constructed previously as part of the work done for my senior project [2]. Initial results showed greater possibilities in parallel imaging. Improvements from this

master's thesis are expected in these parallel imaging capabilities, which will allow faster scan times and possibly reduce motion artifact and reduce patient time spent in the scanner.

In order to perform this research I have improved the 16-channel coil I built previously for my senior design project (see Figure 1.1) [2]. This coil includes eight channels on either side of the neck designed to cover the area between the clavicle and the lower ear. The individual loop elements of these 16 channels cover only half the surface area than the current standard [6] (16 cm^2 compared to 32 cm^2). This will allow higher SNR closer to the surface of the neck, as well as higher SNR at greater depths due to phased array behavior [13,14]. By implementing this design of a phased array of smaller loops, a larger loop element is synthesized by combining these channels resulting in highest SNR near the surface of the coil as well as increased SNR at greater depths as well. Also, by including more channels and maintaining or improving coil sensitivity, the potential for faster imaging using parallel imaging is greater. There were also some necessary mechanical considerations for a practical and ergonomic coil that is easy to use and durable.

The significant contributions of this thesis are to improve patient care by constructing a coil that will aid in acquiring rapid, detailed images of the cervical anatomy, particularly the carotid arteries.

Chapter 2 offers a brief synopsis of MRI background information, covering the basic theory and methods used to acquire images with receive only coil arrays. Chapter 3 provides a description of current coils used for carotid imaging. Chapter 4 is comprised of the paper that is being prepared for submission to the Journal of Magnetic Resonance

in Medicine, which publishes manuscripts describing new developments in MRI research applied to the medical field. Chapter 5 is a conclusion chapter that includes an in depth discussion of the research as well as a summary of the information encompassed in this thesis. This chapter will also include significant conclusions that may lead to continued work in the future.

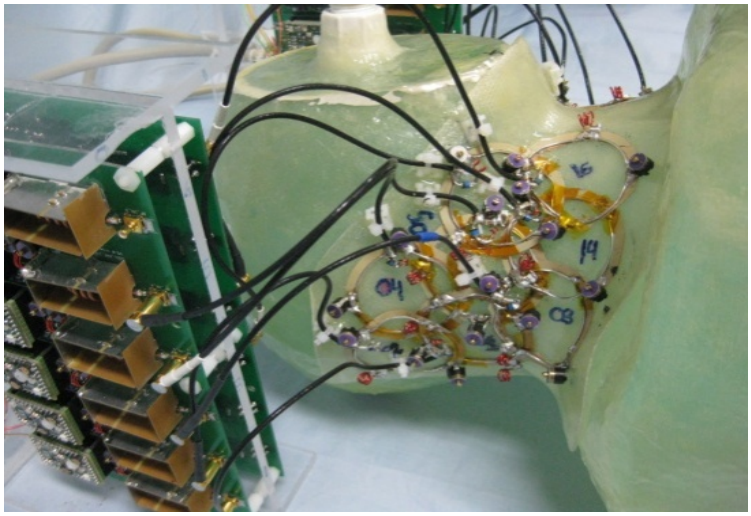

Figure 1.1: New 16 channel coil created to increase SNR and coverage of anatomy of interest.

CHAPTER 2

BACKGROUND

Images produced from an MRI scanner require a complex system of hardware, software, and image reconstruction algorithms. The list of hardware needed for a modern MRI system is extensive, but basically consists of a very large electro-magnet, on the order of 1.5-7 Tesla, with controllable magnetic field gradients and RF fields as well as a computer that provides a control and data review interface. For simplicity the processes of this complex system will be explained in four parts: the magnetic field, producing a signal, acquiring a signal, and processing the signal. The strength of the magnet used for all experiments and studies will be 3T.

2.1 Magnetic field

Of all the elements that can be found naturally in the human body ^{1}H (hydrogen) is the most prevalent. All soft tissue is comprised of significant amounts of this element, due to the abundance of water found in the body. MRI exploits this fact as well as the fact that ^{1}H nucleus (proton) has an inherent magnetic moment. Normally, the random orientation of all of the magnetic moments of the elements in the body produces a net magnetic moment of zero. However, when introduced into a significantly large magnetic field, these nuclei tend to align in the direction of the applied homogenous magnetic field

(***B***), creating a nonzero net magnetic moment. When not aligned with the static magnetic field, the nuclei precess around the axis of the static magnetic field with an angular momentum (ω) proportional to the strength of the magnetic field. The proportionality constant between ω and ***B*** is the gyromagnetic ratio (γ). This ratio is different for the nucleus of each element allowing a frequency distinction between individual elements. The general equation for calculating the precession frequency, also known as the Larmor frequency, is

$$f = \frac{\gamma}{2\pi} B. \tag{1}$$

For ^{1}H (γ = 42.576 MHz/T) the theoretical precession frequency is 127.728 MHz in the presence of a magnetic field with a magnitude of 3 Tesla (T) [1]. For the Siemens Magnetom Tim Trio system used at the Utah Center for Advanced Imaging Research (UCAIR) the frequency of ^{1}H was empirically found to be 123.23 MHz, indicating that the total average magnetic field is slightly less than 3T. There are other magnetic fields that have an effect on this overall average. These additional fields include the gradient magnetic fields, which are used to create a differentiable signal throughout the volume and will be discussed in more detail.

2.2 Producing a signal

The essential purpose of MRI is to accurately but noninvasively obtain an image of the interior of a sample. For this to be possible it is imperative to acquire a high quality signal that contains as much information as possible. At thermal equilibrium, there is no

net magnetization component perpendicular to the axis of the static magnetic field, so there is negligible signal received. In order to use this phenomenon to receive a discernable signal the precessing nuclei need to have the spins tipped into the transverse or axial plane. This is done by applying a radio frequency (RF) pulse magnetic field to the sample. This pulse must have a frequency equal to the Larmor frequency of the element being imaged. If applied transversely, the pulsed magnetic field ($\boldsymbol{B_1}$) tips a component of the magnetization into the transverse plane by a certain angle known as the flip angle (θ). This angle is the angle of rotation from the direction of the main field such that an angle of 0 or 360º will not generate a transverse component.

As the magnetic moment is tipped, the component in the transverse plane precesses at the Larmor frequency as shown in Figure 2.1. The flip angle depends on the strength of the B1 field and the duration of the pulse. The signal is produced as the spins relax back to thermal equilibrium (see Figure 2.1). The time needed for the nuclei to return to equilibrium is an important parameter. This time is separated into the relaxation along the longitudinal (z) axis and the relaxation in the transverse (x,y) plane. These two numbers are designated $\mathbf{T_1}$and $\mathbf{T_2}$ respectively. In order to spatially encode the received signals, external magnetic gradient fields are applied resulting in received signals with unique frequency and phase combinations. These complex signals are contained in a two dimensional (frequency and phase) space called k-space, where each spatial location (voxel) produces a signal with a unique frequency and phase combination. Therefore, with the 2D imaging described in this thesis, the MRI signal is related to a position in a user defined 2Dslice of the object being imaged by a 2D Fourier transform.

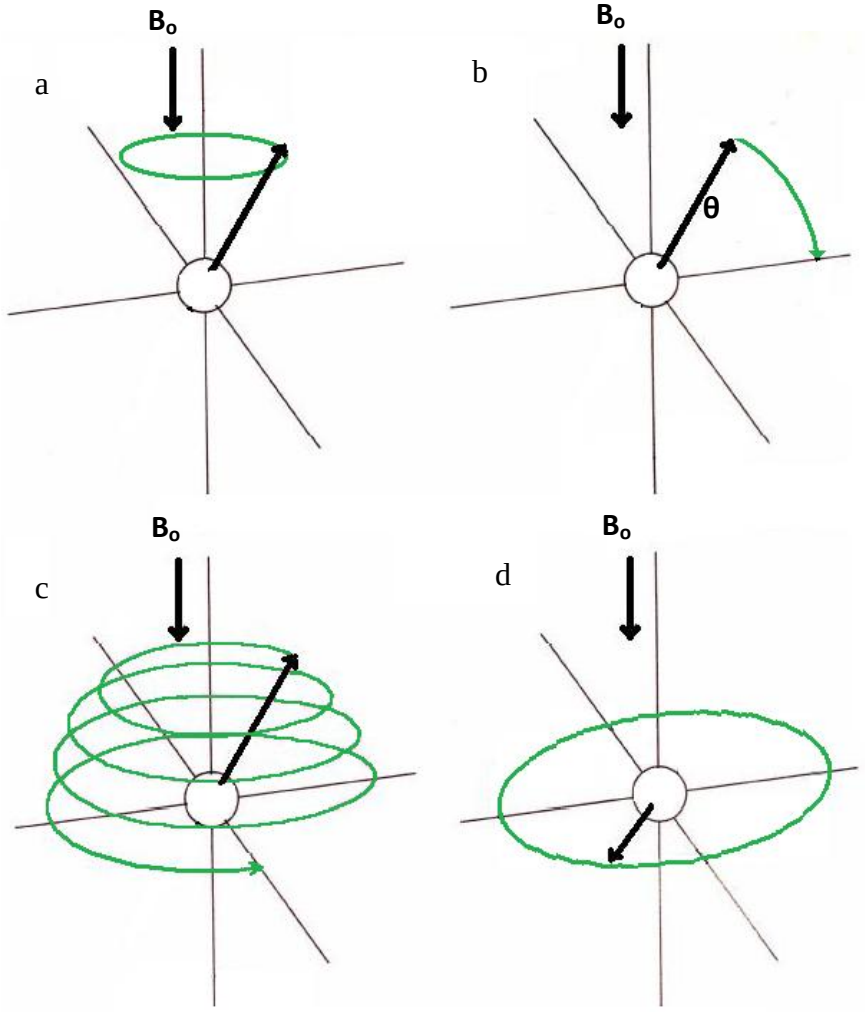

Figure 2.1: Magnetization vectors.
a) shows the vectorized spin of a molecule in a magnetic field b) a molecule whose spin is being tipped into the transverse plane c) the time and position varying precession of molecule with RF pulse d) molecule with spin in transverse (x,y) plane (adapted from [3, 5]).

A complex function that represents the unique frequency-phase combination of each location in k-space may be written as

$$\boldsymbol{g(x,y) = U_x(x,y) + iU_y(x,y)}, \tag{2}$$

By using a bandwidth of frequencies rather than a single frequency the sample can be encoded in one direction by applying a gradient magnetic field in order to vary the frequency linearly along one axis. This axis is often called the read-out (x) gradient. This spatial variation of frequency can be shown by replacing $\boldsymbol{B}$ from (1) with,

$$\boldsymbol{B(x) = B + xG_x}, \tag{3}$$

so that,

$$\boldsymbol{f(x) = \frac{\gamma}{2\pi}(B + xG_x)}, \tag{4}$$

where $\boldsymbol{x}$ is the location in the two dimensional image space, and $\boldsymbol{G_x}$ is the spatially varying $\boldsymbol{x}$ gradient magnetic field. Due to the spatially varying magnetic field resulting from $\boldsymbol{G_x}$, a distinct frequency will be applied to each position $\boldsymbol{x}$ thereby encoding the complex signal.

If the frequency were varied along the y-axis in the same manner, non-differentiable signals would be received in multiple areas. To avoid this, the other axis can be spatially encoded by slightly varying the phase of the signal using another linear gradient. This is usually done by the gradient $\boldsymbol{G_y}$ that is only applied for a short time and is not used during the read-out time (see Figure 2.2). Varying the magnitude of this

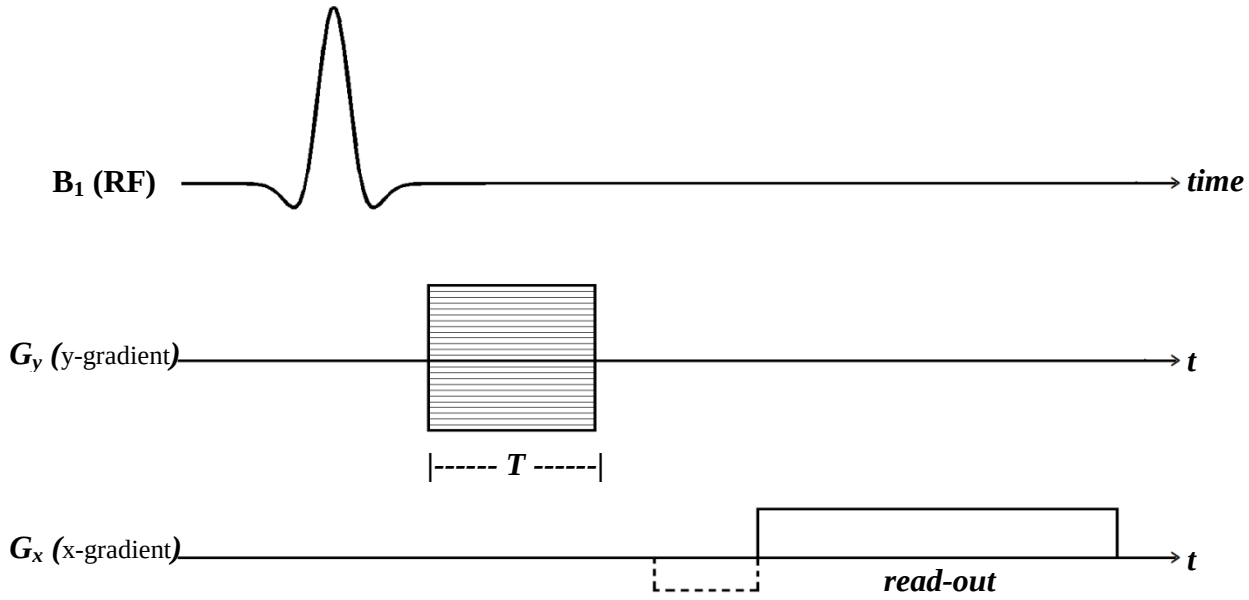

Figure 2.2: A simple example of an MRI timing diagram.
The shaded box of G_y indicates different gradient amplitudes and the dotted line of G_x shows a possible addition to assure that the readout remains consistent

gradient can be thought of as switching lines in k-space. Before each read-out in the ***x*** direction the ***y*** gradient is applied for a specific amount of time ***T*** that effectively moves the line of k-space that is being read into in either the positive or negative ***y*** direction. This produces distinct signals in two dimensions and adds to the encoding of the complex signal by introducing a phase φ which is calculated by multiplying the angular frequency ***ω(y)*** by the duration ***T*** of the applied gradient $\boldsymbol{G_y}$

$$\boldsymbol{\omega(y)} = \boldsymbol{\gamma\left(B + yG_y\right)}, \tag{5}$$

$$\phi(y) = \boldsymbol{T\omega(y)} = \boldsymbol{\gamma BT} + \boldsymbol{\gamma yG_yT}, \tag{6}$$

by adding this phase change to our complex signal the result is

$$g(x,y)e^{-i(2\pi\gamma(B+xG_x)t)}e^{-i(\gamma BT+\gamma yG_yT)}, \quad (7)$$

since $2\pi\gamma B$ and γBT are the carrier frequency and constant phase, respectively, they can be ignored (by mixing the carrier frequency with the desired signal, the resulting signal after demodulation has had the carrier frequency eliminated). Therefore our resulting equation is

$$g(x,y)e^{-i(2\pi\gamma xG_xt)}e^{-i(2\pi\gamma yG_yT)}. \quad (8)$$

We are interested in the entire x-y plane. Therefore, we assume the summation of all signals as shown by

$$\int_{-\infty}^{\infty}\int_{-\infty}^{\infty}\left[g(x,y)e^{-i(2\pi\gamma xG_xt)}e^{-i\,(2\pi\,\gamma\,yG_yT)}\right]dxdy, \quad (9)$$

this complex waveform, once simplified and combined as a complex function, is the 2D Fourier transform of $g(x,y)$ such that

$$F(k_x,k_y)=\int_{-\infty}^{\infty}\int_{-\infty}^{\infty}\left[g(x,y)e^{-i\,2\pi[x(\gamma G_xt)+y(\,\gamma G_yT)]}\right]dxdy, \quad (11)$$

where $k_x=\gamma G_xt$ and $k_y=\gamma G_yT$. With the location of each data point defined in the frequency domain by k_x and k_y this data matrix came to be known as k-space [5].

This spatially encoded signal is important to maintaining a high signal to noise ratio. While these signals originate independent of the MRI coil, the importance of the coil comes from acquiring as much signal as possible while reducing the amount of noise introduced into the system, thus increasing the SNR [14].

2.3 Acquiring the signal

Various different antennas or coils have been built specifically to receive these signals and are designed to work specifically in the near field. There are two main classes of MRI coils. One is a volume coil and the other a surface coil. Their names suggest their primary use. A volume coil usually encompasses the imaging region and provides a very homogeneous signal across the imaging region, but has relatively low SNR. A surface coil can be used to image a region of interest (ROI) that is near the surface, providing relatively high SNR but a very small imaging region. A volume coil and a single element surface coil can have very different applications and each type has unique benefits. However, some of the benefits of a volume coil can also be obtained by using multiple surface coils to synthesize a volume coil. These surface coils are typically arranged into a phased array (PA) in order to maintain the high SNR of the surface coil. Specialized MRI coils are commercially available, but for certain applications it may be best to construct a coil with a specific application in mind [6]. Specific considerations may include the depth and size of the desired imaging region. Specialized coils are then built to fit specific design criteria. These coils are tuned and matched to receive a narrow band of the previously discussed complex signals. The signal is said to be "received" when the spin

of the magnetization vector induces a current on the coil from the alternating magnetic field due to the molecular precession.

2.4 Processing the signal

The small received signal travels through a preamplifier, which amplifies the signal and prepares it to be amplified again by the system. This preamplifier introduces additional benefits during coil construction. Once the signal is processed the data received by the coils are stored in the k-space matrix, the spatial frequency domain, and are then transformed by an inverse 2D Fourier transform and recombined into an image. Generally for physicians this data is quickly transformed by 2D Fourier transform in order to produce an image that can be analyzed. If only one coil element, such as a single element volume coil, is used this transformation is relatively straightforward. Image reconstruction becomes more complicated with the addition of coil elements, so it is necessary to use a recombination algorithm in order to combine the image data. This is often done by the square root of the sum of squares method, but there are several other methods used to combine the data from each channel [14]. For the purposes of this project the method of recombination will be by the square root of the sum of squares. The equation used is as follows

$$A_{im} = \sqrt{\sum_{c=1}^{N} (A_c)^2}, \tag{13}$$

where

$$A_c = \frac{|A|}{\sigma_{noise}} \tag{14}$$

and A_{im} is the complex image data matrix for an individual channel, σ_{noise} is equal to the standard deviation of the noise received by the coil, c is the channel number, N is the number of channels, and A_{im} is the resulting rSNR matrix of a particular slice. Therefore, for a coil containing 16 channels (N=16) the resulting matrix A_{im} would be a combination of all 16 coils and would be the same size as an individual channel matrix.

CHAPTER 3

COIL DEVELOPMENT

Development of the 16-channel RF coil and comparison with the standard RF coil used for imaging the carotid arteries.

3.1 Current four-channel standard

Currently the standard for quality MR imaging of the carotid artery is a four-channel bilateral coil. This coil provides many advantages over other commercial coil designs. The greatest improvement over other coils is the increased SNR [6]. With this four-channel coil, the relative SNR was significantly increased at the carotid bifurcation. One limitation of this coil is that it provides coverage only over a small extent of the anatomy of interest, resulting in a smaller field of view (FOV). It happens regularly that when a patient is scanned for the purpose of imaging their bifurcation, the bifurcation is not located in the FOV of the coil. In this case the coil needs to be repositioned relative to the patient, which can lead to an increase in the time and cost of the scan. Also, due to the great variety in the anatomy of each individual neck, sometimes there is significant separation between the coil and the patient, which leads to a reduction in SNR. Overall this particular coil design has greatly improved carotid imaging, but we will seek to

further improve the design with the modifications presented in this thesis. These improvements will be quantified by measuring results obtained with different coils.

3.2 Six- and eight-channel carotid coils

A six-channel coil designed to image the carotid bifurcation was presented at the ISMRM conference in 2004 [7]. This coil consists of two sets of three circular loop elements symmetrically overlapped. This paper unfortunately did not make a direct comparison to any of the carotid coils that were available for my work. However, the coil showed a 73% improvement in SNR over a commercially available neck coil at a depth of three and a half centimeters. Due to the limited number of coil elements, this coil is also inherently limited in its potential for parallel imaging.

To date the carotid coil with the most channels, other than the one described in my work, is an eight-channel coil available from the Hayes research group at the University of Washington [8,9]. Their design addresses the issue of limited anatomical coverage of the four-channel coil. The modification to this design was to double the size of the coil by adding an additional pair of bilateral coils to each side of the neck, resulting in a coil configuration consisting of eight channels in total. Each set of four elements consists of a set of two elements overlapped left to right that are then overlapped by an identical second set in the superior/inferior direction. This design was published in the fall of 2009, and an interesting note is that this same design was independently considered for the purposes of this project prior to the publication of that work. The publication of the eight-channel coil shows a significant improvement in SNR at the carotid bifurcation compared to the previously mentioned four-channel coil. A 90%

improvement was measured at a depth of five centimeters with a 70% improvement at a depth of three and a half centimeters. While these findings are significant, the greatest improvements come at depths deeper than the average bifurcation (3 1/2 cm). Also, this design does not conform well to the anatomy being imaged. For example, a person with a short neck would not fit comfortably in this coil. It is anticipated that by adding even more channels, the parallel imaging performance could be improved.

3.3 Improvements to existing designs

At the outset of this work an eight-channel design, similar to that described above [9], was considered. Simulations were done to show the expected sensitivity profile for loops overlapped in the z direction, or along the length of the magnetic bore, which is the direction of the magnetic field. These simulations determined the overlap distance needed for the compensating overlap, which would improve the coil sensitivity profile in the ***z*** direction (see Figure 3.1). One problem with this simulation was that only one point of each loop was considered, so the resulting calculations were simplified but in a rectangular loop model this produces a good approximation [14]. A model was built and empirically tested for two overlapped coil elements. During this process the circular loop design was also considered. It was determined that it would be more feasible to better fit the anatomy of interest closely by using smaller diameter circular loops rather than implementing the rectangular loop design. The reduced loop size would also allow more elements to be placed near the anatomy of interest, and would therefore increase the parallel imaging capabilities of the coil [16]. Because of the movement associated with this region of the body (breathing, swallowing, and pulsatile blood flow), there is room

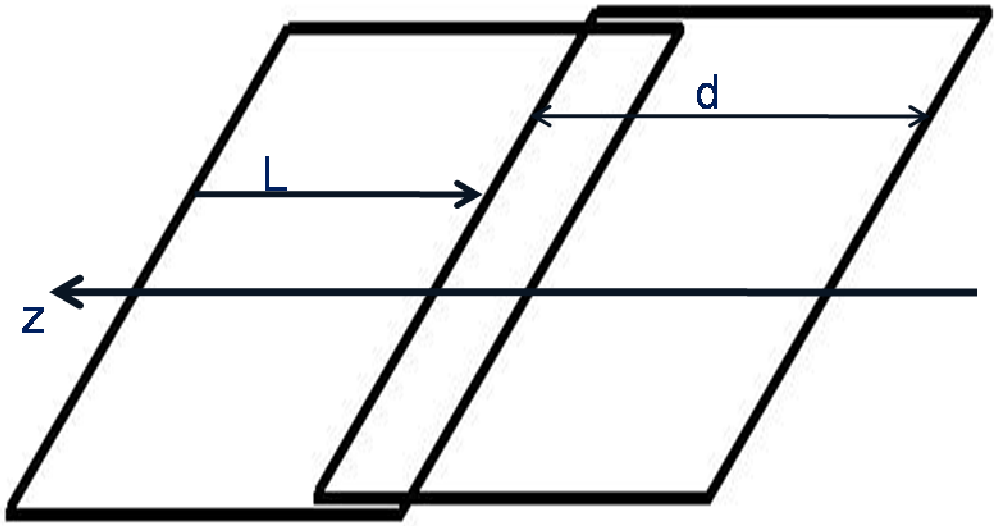

Figure 3.1: Overlapping of rectangular loops with a compensating overlap. A perfect overlap occurs when L=0.9*d and compensating occurs when L<0.9*d

for improvement in image quality. There would be clinical benefits if discrimination of small plaque morphology were possible with the highest SNR attainable.

The method actually implemented in this thesis is more similar to a design for a coil to image the optic nerve in the brain [10,11]. This design used a cluster array pattern similar to that which will be described in the following section. However, smaller loop sizes were used because the carotid arteries are not as deep as the optic nerve [13]. This design method was used for optic nerve imaging partly because it provides high SNR over a wide range of depths. This is possible because the smaller loop elements receive data that can be combined in such a way that the loops synthesize a larger loop in the depth of penetration of the coil sensitivity profile, but the higher SNR of smaller loop elements is still maintained [15]. Due to the large variations from patient to patient in the location of the carotid bifurcation, the desired outcomes of this thesis work needed a specialized coil that could obtain high SNR over a large volume.

Also, it was important to build a former for a coil that would fit most people being scanned for carotid disease. A volunteer was found whose expressed physical characteristics matched those of a "typical" carotid patient, and who could be modeled for a former size as well as a phantom design. The phantom needed to represent the human anatomy more accurately than a simple cylindrical phantom. A head-neck-shoulders phantom was built and filled with a homogenous copper sulfate solution [4].

In trying to find a way to precisely show the advantages of the new 16-channel carotid coil over the four-channel coil it was decided to compare the SNR along the length of the carotid vessel. This means the SNR would be recorded starting at the circle of Willis in the brain and then at 5 millimeter increments along the internal carotid artery down through the common carotid until it reaches the aortic arch. Assuming, for the phantom comparisons, that the internal carotid artery is contained in a single sagittal plane; results of testing and comparison have shown significant improvements in the 16-channel carotid coil over the four-channel coil. For example, the 16-channel coil provides an average improvement in SNR in the phantom of 128%, 87% and 71% along sagittal planes that represent an artery that varies in depth from 3-6.2 cm, 4-7.5 cm or 5-8.3 cm, respectively. When comparing the two SNR profiles by their full width at half max, the 16-channel coil has a range of 10 cm while the four-channel coil is limited to 8 cm. Also, when compared to the peak SNR of the four-channel coil, the 16-channel coil maintains or improves this four-channel peak value over a distance of 10 centimeters.

In summary the new 16-channel coil design will improve patient care by providing healthcare professionals with higher quality images over a larger superior to inferior extent of the carotid artery. This also includes the ability to image more quickly,

which reduces the effects of patient motion on the images. Because of the great variability in carotid artery disease, it is important that signs of disease can be recognized early. This can be done more easily with higher quality images, especially if these higher quality images are available for larger volumes.

The International Society for Magnetic Resonance in Medicine is the most recognized society that is directly related to this research. The opportunity to present research at one of their international conferences is a privilege. The requirement for proposal submission to the ISMRM annual conference held in Stockholm, Sweden in May of 2010 was a one page abstract. I wrote and submitted an abstract, which was accepted for the presentation of an electronic poster [12], and I also received an Educational Stipend from the society, which waived my registration fees. This stipend was offered to a limited number of students. I was able to attend the conference and present my research. My presentation primarily dealt with the comparisons that were made between the four-channel bilateral phased array carotid coil and my 16-channel bilateral phased array carotid coil. The opportunity was very rewarding and very educational. A paper more fully describing the information presented at this conference is being prepared that will be submitted to a major MRI journal. The paper will show the comparisons between the two coils as well as some data showing the improvements in parallel imaging.

CHAPTER 4

INCREASED VESSEL DEPICTION OF THE CAROTID BIFURCATION WITH A SPECIALIZED 16-CHANNEL PHASED ARRAY COIL AT 3T

4.1 Increased Vessel Depiction of the Carotid Bifurcation with a Specialized 16-Channel Phased Array Coil at 3T[1]

Quinn Tate, BS[1,2], Seong-Eun Kim, PhD[2,3], Gerald Treiman, MD[3,4], Dennis L. Parker, PhD[2,3] , J. Rock Hadley, PhD[2,3]

1. Department of Electrical and Computer Engineering, University of Utah
2. Utah Center for Advanced Imaging Research
3. Department of Radiology, University of Utah
4. VA Hospital, Salt Lake City, Utah

Abstract

The purpose of this work was to design and construct a multi-channel receive-only RF coil for 3 Tesla magnetic resonance imaging of the human carotid artery and bifurcation with optimized signal to noise ratio in the carotid vessels along the full extent of the neck. A neck phantom designed to match the anatomy of a subject with a thick short neck, representing a body habitus often seen in subjects with carotid arterial disease, was constructed. Sixteen circular coil elements were arranged on a semi-rigid fiberglass former that closely fit the shape of the phantom, resulting in a 16-channel bilateral phased array coil. Comparisons were made between this coil and a typical 4-channel carotid coil in a study of 10 carotid vessels in 5 healthy volunteers. The 16-channel carotid coil showed a 70%averageimprovement in signal to noise ratio (SNR) at the carotid bifurcation. This coil also maintained an SNR greater than the peak SNR of the 4-channel coil over a vessel length of 10 cm. The resulting increase in SNR improved vessel depiction of the carotid arteries over an extended field of view, and demonstrated better image quality for higher parallel imaging reduction factors compared to the 4-channel coil.

Introduction

Disease in the cervical carotid artery is a major cause of stroke and subsequent disability and mortality. With an annual estimate of more than 100,000 deaths per year, stroke is the third leading cause of death in the United States [1]. Cardiovascular magnetic resonance imaging (MRI) is a safe and noninvasive method that adds crucial information to that obtained by conventional Doppler ultrasound. Adding to this information is a significant amount of published literature of various MRI techniques used to accurately identify the vessel wall and characterize constituents of plaque [2-6].Unfortunately, in clinical practice, the diagnostic utility of MRI as applied to the examination of atherosclerotic disease is reduced because of artifacts, inadequate tissue contrast, reduced signal to noise ratio (SNR), and patient-dependent factors such as body habitus or inability to remain motionless for the length of the scan [7]. Due to the very small (0.1 to 0.5mm) size of some important details in carotid plaques, the images should be acquired with high spatial resolution [8]. Unfortunately, there is a difficult trade-off between voxel

[1] This manuscript has been submitted to The Journal of Magnetic Resonance in Medicine

size and image SNR. Imaging with small voxels (high spatial resolution) can require longer scan times in order to maintain adequate image SNR. The new generation of MRI scanners operating at a magnetic field strength of 3T has demonstrated a number of advantages for carotid plaque imaging including an increase in available SNR. This corresponds to improved spatial resolution, and reduced scan time [9].

In order to more fully utilize the available SNR, it is essential that the coil array be designed to cover the region where arterial disease is most likely to occur. It has been reported that vessel geometry and hemodynamic forces are major factors contributing to the development of vascular pathology including plaque deposition [10,11].In regions of low wall shear stress due to blood recirculation and stasis, there is an increased chance of atheroma deposition [6-8]. Such regions are found around vessel bifurcations, where the blood flow is disturbed [5]. However, the location of atherosclerotic plaques in the carotid arteries are not limited to the bifurcation, but can also be found several centimeters in either the superior or inferior direction [6,12]. Also, the relative location and geometry of the bifurcation of the common carotid artery to the internal and external carotid arteries varies from patient to patient and can vary in the same patient bilaterally. The distinct inter- and intra-patient variations in vasculature result in an extended region of interest with the location of the bifurcation ranging from the lower ear to just above the clavicle at an average depth of 2-5 cm.

A significant increase in SNR can allow for shorter scan times, which could potentially reduce artifacts from vessel motion caused by respiration, swallowing and pulsatile blood flow. Recently, parallel imaging techniques have been used for a study of carotid atherosclerosis imaging using a specialized 4-channel carotid coil and the GRAPPA parallel imaging acquisition and reconstruction technique [13]. There are several techniques that have been developed to accelerate signal acquisition and reduce scan time [14,15]. Parallel imaging techniques rely on the RF coil sensitivity profiles of an array of coil elements to reconstruct images from under-sampled measurement data. Under-sampled data is faster to obtain, but has lower intrinsic SNR due to fewer samples included in a given image. Parallel imaging does not recover SNR, but does utilize coil sensitivity to make up for missing k-space measurements. Parallel imaging combines the signals of several coil elements in a phased array in order to reconstruct the image. An objective of parallel imaging is to accelerate image acquisition speed and reduce scan time. Although implementing parallel imaging techniques in carotid MRI may improve the overall imaging quality by reducing artifacts, parallel imaging does reduce the available image SNR. Unfortunately, parallel imaging of the carotid bifurcation is a method for which no carotid coil has yet been optimized due to the limited number of coil elements in the available four, six and eight channel carotid coils. Parallel imaging performance can be determined by the available SNR of the coil array, the number of coil elements used, and their relative geometric positions [15,23-24].

To improve image quality in high-resolution MRI using parallel imaging, it is crucial to increase the available SNR. Due to the variation in the bifurcation

position relative to the specific patient anatomy, it is also important that the area of coil coverage is large enough to include the region most likely to contain the bifurcation. A carotid coil whose sensitive region will cover most positions of the carotid bifurcation will extend from near the aortic arch to the level of the ear in the S/I direction. A phased array coil with an extended sensitivity region that will also result in higher SNR over this volume being imaged is fundamental to improving image quality of the carotid arteries.

Increased coverage is necessary, not only because of the variation in position of the carotid bifurcation between patients, but also due to the variation in disease location relative to the bifurcation. It is possible to trade high SNR for acceptable SNR with either parallel imaging or high resolution. High spatial resolution, for disambiguation of plaque components, is key in early detection of potential stroke patients. Therefore, an increase in image SNR along the full extent of the carotid vessels will provide significant benefit by improving quality, reducing scan time or increasing resolution. There is also the possibility of moderate improvement in high definition images while increasing the speed of image acquisition with parallel imaging.

There are limitations in the coils that are currently used for carotid MRI. Neurovascular coils that are designed with a small number of large elements can provide coverage along the entire length of the carotid artery but achieve limited SNR [9]. As explained by Wright et al.[16], increasing the number of receiver elements surrounding the volume can yield increased SNR near the coil elements as long as the coil elements remain sample noise dominated as opposed to coil noise dominated [20]. The increased number of elements maintains coil sensitivity at greater depths [16]. A4-channel(bilateral 2-element arrays) [9,17] phased array (PA) surface coil [21] achieves the highest SNR directly beneath the coil elements.This 4-channel coil has been used in numerous studies at our institution and for several years has been considered the current standard [9]; however, the design is one that has a limited FOV and can require repositioning of the coil, relative to the patient, in order to center the coil over the location of the carotid disease. Modifications to this design have been made in order to optimize and extend the FOV [9,18]. These modifications, while increasing the coverage of the coil, may still require repositioning of the coil relative to the patient [9]. A recently developed 8-channel carotid coil has been shown to significantly increase rSNR at the bifurcation (70%) as well as increase the FOV of the coil, when compared to the standard 4-channel coil. However, the increase in S/I FOV coverage for a constant rSNR value through a phantom image is limited to 6 cm [19].

The goal of this work was to develop a specialized receive only phased array (PA) carotid coil that would improve the SNR and extend the region of coil sensitivity, particularly in the S/I direction. In addition, it was desired to increase the parallel imaging performance with the use of an increased number of coil elements. The result was a custom coil composed of 16 circular loop elements placed on a close fitting fiberglass former (16ch). This work presentsdetails on the phantom and coil design and construction, as well as the comparison results

between imaging performance characteristics of the 16ch and standard 4-channel (4ch) recieve only RF carotid coils (see fig. 2).

Methods

In this work, carotid coil comparisons were made using both studies from a homogenous phantom as well as in-vivo human carotid studies. All studies were performed using a Siemens 3T TIM Trio MRI scanner (Siemens Medical Solutions, Erlangen, Germany). IRB approval was obtained for all studies described in this work and patients gave their informed consent.

Phantom Construction

In conjunction with the 16ch carotid coil, a custom fiberglass phantom was constructed to represent the head, neck and shoulder of the human anatomy. The phantom, modeled after a volunteer whose expressed physical characteristics were similar to those of many of the patients with carotid arterial disease imaged at our institution, was constructed of fiberglass thick enough to be rigid. In addition to providing a homogenous volume through the sensitive region of the 16ch coil, the phantom also offered a more accurate load for the coil elements than would have been achievable with a simple cylindrical phantom. The phantom was filled with a homogenous aqueous copper sulfate solution containing 1.955g $CuSO_4$ $5H_2O$ per liter of water. Salt was then added to the solution to empirically adjust the conductivity and achieve comparable coil loading to that of a human subject.

Coil Construction

In order to achieve the goals of this work, and create a close fitting ergonomic coil former, it was decided to use circular loop elements for the 16ch coil. On average, the expected imaging depth for the carotid bifurcation is 2-5 cm with an average depth of approximately 3 cm [9]. At 3T, considering proton imaging, a design consisting of multiple loops with a diameter of 4.5 cm [20] was used to improve the SNR at shallow depths, due to the small size of the individual elements. Improvements in SNR at greater depths (>3 cm) were expected due to the synthesis of the smaller loops to form larger loops as a result of multi-channel reconstruction algorithms. The schematic for individual coil circuitry is summarized in Figure 3.

The coil former was designed to cover the neck from the lower ear to just above the clavicle. This allowed coil element placement that could provide high signal sensitivity over the majority of potential carotid bifurcation positions. This former was made of fiberglass with a thickness that resulted in a semi-rigid structure. Eight coil elements were placed on each side of the neck and were arranged in geometric pattern, resulting in reduced coupling of adjacent coils [21-22], on each side of the former for a total of sixteen elements. Each element was made from 18-gauge wire with 4 equally spaced capacitors (see Figure 3). Each coil element was connected to its own pre-amplifier by a 24 cm coaxial cable in series with a phase shifter network and a cable trap that was used to reduce common mode currents and unwanted coupling between individual coil cables.

Coil Comparisons

All carotid coil comparisons were made between the new 16ch carotid coil and a slightly modified version of a widely used 4-channel receive PA coil design published by Hayes et al. [17]. The 4-channel coil comprised of two bilateral paddles, each consisting of two overlapped rectangular loops (e.g. 4.5x4.5 cm) [21]. The modifications to the Hayes 4-channel coil were slightly elongated loops in the S/I direction (7x4.5 cm) in order to increase the coil coverage along the length of the vessels. Figure 2b displays the modified 4-channelcoil (4ch) used in this study.

Coil comparisons consisted of phantom studies to assess relative SNR (rSNR), where the term 'relative' is used to make reference to the assumption that all other factors, besides variations in the coils themselves, are held constant and that it is the magnitude of received SNR that is compared. Human studies were used to assess how the coils affected clinical images by evaluating arterial rSNR profiles and parallel imaging performance.

Phantom Studies

An rSNR comparison of the 16ch and 4ch coils was performed using the custom phantom. The results of this study, produced rSNR images [15] whose SNR levels could then be compared at specific depths. Depth and length measurements were taken from the positions of 12 carotid bifurcations from existing de-identified patient data in order to make reasonable depth and position rSNR comparisons in the phantom. The resulting average depth was used (4.2 cm), along with two other depths that more closely characterized the extremes (3cm and 5cm). Axial, coronal and sagittal slices were selected from stacks of 2D phantom images that most closely corresponded to these measurements (see Fig. 4a). The corresponding phantom measurements were centered at the most narrow portion of the phantom neck which was estimated to be the most common position of the carotid bifurcation in the S/I direction. Also, the carotid arteries were assumed to be contained in a single sagittal plane, such that the reported depth is the separation between the coil and the carotid bifurcation at its most shallow depth (see Fig. 4a). Because the depth of the carotid artery in a human neck varies significantly along the length of the neck [9], the corresponding assumption of the artery being contained in a single sagittal plane resulted in a depth ranging from 4.2 cm to 7.5 cm along an S/I length of 10 cm (see Fig. 4a).

The data acquired from the phantom studies provided a homogenous comparison between coil sensitivity profiles. Because the phantom was modeled after a human, measuring a constant distance from the contour of the phantom did not provide useful information. However, by assuming the arteries to be contained in a single plane it was possible to make comparisons in three different planes with varying depths. The depths chosen for assumed bifurcation depth were 3, 4.2 and 5 cm. The phantom studies also provided the data needed to determine and analyze the parallel imaging capabilities of the two coils [24].

Human in-vivo Studies

For the in vivo carotid artery rSNR profile comparisons, 5 healthy volunteers with varying neck sizes and bifurcation positions were included. In order to compare coil rSNR profiles of the 16ch and 4ch coils along the axis of

the carotid vessels over the full extent of the neck, a 2D TOF sequence was used with the following parameters: 60 slices, TE/TR = 5.5ms/27ms, FOV = 30x30cm^2, Matrix = 512x512, FlipAngle = 50^o, and slice thickness = 5mm. Imaging studies for each volunteer were performed on the same day using both the 16ch and4ch coils. The rSNR from 10 carotid arteries was compared over a volume with an S/I length of 30 cm.

These data were used to calculate the rSNR for each individual channel by dividing the signal intensity of the image by the standard deviation of the noise in the image background (air region with no signal or artifact) throughout the volume. The different channels were then combined using the square root of the sum of squares algorithm [21]. For each reconstructed image slice, ROI's were drawn around the internal carotid, bifurcation, or common carotid artery and the signal intensities for all voxels within 60% of the peak value inside the lumen were averaged. The average axial vesselrSNR values obtained at each 5mm increment along the artery were plotted for both coils. The data provided axial rSNR values from the circle of Willis along the internal carotid artery, through the bifurcation and along the common carotid artery to the aortic arch. Each individual rSNR profile was spatially aligned so that the bifurcation of each profile was centered at 0 cm. Also, the standard deviation of the group was shown by adding error bars to the averaged data.

For comparisons of image quality using parallel imaging techniques with both the 16ch and 4ch coils, a 2D TSE sequence was used to produce a volume of 2D T2w images using GRAPPA [23] with a reduction factor of 2(R=2). The sequence parameters were as follows: 24 axial slices, TE/TR = 64ms/3500ms, ETL = 11, FOV=13x13 cm^2, matrix = 256x256, slice thickness=2mm,withfour averages. To compare the quality of high-resolution images, a 3D T1w TSE sequence was used with 32 slices, TE/TR=23ms/700ms, ETL=37, EchoSpacing=5.2ms, FOV=14x14 cm^2, matrix = 640x640, slice thickness =1.0 mm, and voxel size=0.22x0.22x1.0 mm^3.The same imaging parameters were used for scans performed with the 4ch and the 16ch coils. As a reference, one of the volunteers was also scanned, with the same acquisition protocols, using the body matrix coil and then again using the Siemens 19-channel head/neck matrix used for cervical artery and head imaging (this 19-channel array is commonly used for clinical imaging of stroke patients).

Results

Phantom Studies

Figure 4 displays rSNR images acquired from a homogenous solution, to show the loss in signal with increasing depth or distance from the coil. These phantom studies demonstrated a significant increase in rSNR, from the 16ch over the 4ch, at depths close to the coil surface. The percent improvement, 16ch rSNR divided by the 4ch rSNR, decreased with increasing depth. The average rSNR improvement from the 16ch coil over a distance of 10cm in the deep carotid plane, depths ranging from 5 to 8.3 cm, of a single sagittal slice was more than a 70% increase over the 4ch rSNR. The average rSNR improvement over a distance of 10 cm in the shallow carotid plane, depths from 3 to 6.2 cm, resulted in more than 125% improvement of the 16ch over the 4ch.The plots in Figure 5

contain rSNR data from both a transverse and longitudinal cross section of the coronal image from figure 4. These plots show there is a significant improvement in the rSNR profile in the S/I direction and with increasing depth. For example, relative to the peak rSNR of the 4ch the 16ch coil maintained or increased the rSNR over a simulated vessel length of 10 cm.

There were also improvements in the parallel imaging capabilities as shown by the 1/g factor maps (see fig. 4b). The relationship between SNR (rSNR) and the g factor is shown by the following equation

$$\mathrm{SNR_{PI}} = \frac{\mathrm{SNR_{full}}}{g\sqrt{R}}$$

where SNR_{full} is the result of using all k-space data and SNR_{PI} is the magnitude of rSNR acquired by sub-sampling k-space by implementing parallel imaging and R is the reduction factor [17]. A plot of one over the g factor demonstrates the losses that occur by implementing parallel imaging in a given direction. While these maps show that it is theoretically possible to have a reduction factor equal to four (R = 4) for the 4ch coil, this can result in an additional loss in rSNR of nearly 50% (1/g < 0.5) [17].

In-vivo Human

Figure 6 compares the axial vessel rSNR along the axis of the carotid vessels, from the Circle of Willis to the aortic arch, between the 4ch and 16ch coils. The mean rSNR profile for each coil is shown with the associated standard deviation error bars. Note that while the lower limit of the standard deviation of the received rSNR from the 16ch coil extends below the upper limit of the standard deviation of the rSNR of the 4ch coil, the 4ch never outperformed the 16ch coil in any given study. The lower rSNR limits for both coils were obtained when imaging a subject with deeper arteries and the upper rSNR limits were obtained while imaging shallow arteries. The trends observed in the phantom rSNR studies were also observed in the human studies.

Also plotted in Figure 6 are the rSNR measurements obtained using the 19-channel head/neck imaging matrix coil. There was an increase in rSNR at the bifurcation for an appropriately positioned 4ch custom coil, which confirms previous literature [9-11]. However, when comparing the coverage of the 4ch and 19-channel array, the 19-channel provides more consistent rSNR over the full length of the carotid vessels, from the Circle of Willis to the aortic arch. In contrast, the 16ch coil provided comparable coverage to the 19-channel coil while significantly improving the rSNR in the region of the bifurcation.

There were also improvements in parallel imaging with the 16ch compared to the 4ch coil. Figure 7 displays the 2D T2w images of a subject who had visible disease. These images were acquired with the 4ch and 16ch coils while using a parallel imaging reduction factor of two (R=2). For R=2 the 4ch introduces a noticeable reduction in image quality. Images from the 16ch at the same reduction factor show that near the center of the image, where the improvements in rSNR were not as significant, there is minimal loss in image quality. However, inspection of the images in the regions closer to the skin surface, near the bifurcation, shows a noticeable improvement in image quality, both in rSNR and contrast, over the images acquired using the 4ch coil. The improved 16ch image

quality results in increased definition of the vessel wall and various plaque components compared to the 4ch images. Figure 8 shows clinical images using the 16ch coil with different reduction factors (R=1,2 and 4) compared the 4ch coil with R=2.

The increase in rSNR of the 16ch coil can also be used to obtain increased image resolution while maintaining and possibly improving image quality. Figure 9 displays 3D high resolution T1w images acquired using the 16ch and 4ch coils. Inspection of these images shows that in 3D high resolution (0.22x0.22 mm^2 in plane resolution) imaging the overall image quality, including reduced background noise and increased image clarity, is improved with the 16ch coil based upon visual inspection.

Discussion

The design of the 16ch coil greatly increased the received rSNR over the 4ch coil along the entire length of the carotid vessel. From the comparison at the bifurcation, where there is often significant signal loss due to disordered, non-repetitive blood flow, there is an average improvement of 70% in rSNR using the 16ch coil. The analysis of the data acquired using a phantom shows that the 16ch provides an appreciable gain in rSNR with increasing depth compared to the 4ch coil. The increase in rSNR is evident along the entire length of the carotid artery. On average, nearly twice (1.98) the available SNR was received over a range of eight centimeters centered at the carotid bifurcation. The improvement in rSNR received by the 16ch over the peak rSNR of the 4ch extends for 10 cm along the length of the vessel. This demonstrates that the 16ch has a much greater likelihood of being sensitive to the region containing the carotid bifurcation, reducing the need for coil repositioning that is often required when using the 4ch coil.

This increase in rSNR allows for improved parallel imaging performance and potential reduction of motion artifacts [25], as well as high definition imaging with improved vessel definition. If the reduced scan time achieved using the 16ch coil with parallel imaging can consistently produce images comparable to those acquired with the 4ch coil during a full-length sequence, clinical throughput could be greatly improved. Future work will investigate the clinical tradeoffs between increased rSNR and image acquisition speed as well as other benefits of using parallel imaging as part of carotid vessel imaging protocols. The high definition images (see fig. 8) may allow for a more in depth study of plaque composition. Also, the improvement in 16ch rSNR may also be advantageous in new methods of motion correction such as in the work done by Mendes et al. [25] for reasons similar to those of improvements with parallel imaging. Studies are currently being performed to determine the clinical significance of these applications.

The scanner used for these studies is equipped with a total of 32 channels. The additional channels available on the Trio scanner might also be used in combination with the 16ch coil in order to provide a more complete imaging region including the entire carotid artery from the Circle of Willis to the aortic arch possibly including coverage of the head. Currently there is a head/neck support available which contains 4 additional coil elements that has been used in combination with the 16ch coil. These additional elements provide

improved image quality over the region of the neck and in particular the cervical spine. However, the clinical benefit of these elements for carotid imaging is yet to be determined.

Even though the 16ch coil former was not optimized for all patient neck sizes or for all anatomical locations of the bifurcation, the coil performed well for the wide variety of patient anatomy involved in this study. In order to accommodate a larger percentage of possible patients, more than one former size may be needed. Other options include the division of the coil former into two sections. This would allow a single coil to be used for a wider range of neck sizes.

A benefit of the 4ch coil is that it has the flexibility to be placed virtually anywhere, regardless of patient anatomy. For the cases of unusual bifurcation position, the 16ch coil is limited in that the semi-rigid former may not allow the coil elements to be placed in a specific location. In these instances, the 4ch coil might outperform the 16ch coil in rSNR. Also, this study focused on centering the 4ch coil over the carotid bifurcation, if a diseased area were located somewhere away from the bifurcation, it may be possible that the 4ch coil would provide a more apt solution. However, if the 16ch coil former were to be divided into two sections to fit a wider variety of patient body habitus the flexibility in 16ch positioning would be improved. Another limitation of the current 16ch design is the cumbersome pre-amp housing and assembly that is in close proximity to the head of the patient. Future work will include the design of a more ergonomic and patient friendly design allowing for the close proximity of the pre-amps, circuit boards and associated RF circuitry.

Conclusion

A specialized 16ch PA coil for imaging the carotid bifurcation was designed to increase coil rSNR and to extend vessel coverage of the carotid artery as compared to an in-house 4ch PA carotid coil. The 16ch coil significantly surpassed the 4ch coil in both coil coverage and rSNR. The 16ch coil showed an average improvement of more than 70% in rSNR at the bifurcation while the average improvement ±4 cm distance from the carotid bifurcation was greater than 100% improvement over the 4ch coil. The 16chcoil maintained an rSNR improvement over the 4ch along the entire length of the carotid artery from the Circle of Willis to the aortic arch, when the bifurcation was located near the center of the neck, and demonstrated substantial improvements in parallel and high resolution imaging when compared with the 4ch coil.

Acknowledgements

- Ben B. & Iris M. Margolis Foundation
- Clinical Merit Review Grant from the Veterans Administration Health Care System
- NIH R01-HL057990
- Siemens Medical Solutions
- Melody Johnson, Henry Buswell and Anne Haroldsen

References

1. Xu J, Kochanek KD, Tejada-Vera B. Deaths: Preliminary Data for 2007. National Vital Statistics Reports 2009;58:1-5

2. Yuan C, Mitsumori LM, Ferguson MS, Polissar NL, Echelard D, Ortiz G, Small R, Davies JW, Kerwin WS, Hatsukami TS. In vivo accuracy of multispectral magnetic resonance imaging for identifying lipid-rich necrotic cores and intraplaque hemorrhage in advanced human carotid plaques. Circulation 2001;104:2051
3. Hatsukami TS, Ross R, Polissar NL Yuan C. Visualization of fibrous cap thickness and rupture in human atherosclerotic carotid plaque in vivo with high-resolution magnetic resonance imaging. Circulation 2000;102:959
4. Corti R, Zahi AF, Fuster V, Worthley SG, Helft G, Chesebro J, Mercuri M, Badimon JJ. Effects of lipid-lowering by simvastatin on human atherosclerotic lesions
5. Glagov S, Zarins C, Giddens DP, Ku DN. Hemodynamics and atherosclerosis: insights and perspectives gained from studies of human arteries. Arch Pathol Lab Med 1998;112:1018-1031.
6. Rutherford R B. “Vascular Surgery”. 2005 Elsevier Inc.
7. Wallis de Vries BM, van Dam GM, Tio RA, Hillebrands JL, Slart RH, Zeebregts CJ. Current imaging modalities to visualize vulnerability within the atherosclerotic carotid plaque. J Vasc Surg 2008;48(6):1620-1629
8. Fayad ZA, Fuster V. Clinical imaging of the high-risk or vulnerable atherosclerotic plaque. Circ Res 2001;89:305-316.
9. Hadley JR, Roberts JA, Goodrich KC, Buswell HR, Parker DL. Relative RF coil performance in carotid imaging. Mag Res Imag 2005;23:629-639.
10. Ku DN, Giddens DP, Zarins CK, Glagov S. Pulsatile flow and atherosclerosis in the human carotid bifurcation—positive correlation between plaque location and low and oscillating shear stress. Ath Atherosclerosis 1985;5:293–302
11. Glagov S, Zarins CK, Giddens DP, Ku DN. Haemodynamics and atherosclerosis—insights and perspectives gained from studies of human arteries. Arch Pathol Lab Med 1988;112:1018–1031.
12. Moore WS, Hall AD. Importance of emboli from carotid bifurcation in pathogenesis of cerebral ischemic attacks. Arch Surg 1970;101(6):708-711 passim.
13. Saam T, Raya JG, Cyran CC, Bochman K.High resolution carotid black-blood 3T MR with parallel imaging. J of Cardiovascular Mag Reson 2009;11:41
14. Sodickson DK, Manning WJ. Simultaneous acquisition of spatial harmonics (SMASH): ultra-fast imaging with radiofrequency coil arrays. MRM 1997;38:591-603.
15. Pruessman KP, Weiger M, Scheidegger MB, Boesiger P. SENSE: Sensitivity Encoding for Fast MRI. MRM 1999; 42:952-962
16. Wright SM, Wald LL. Theory and application of array coils in MR spectroscopy. NMR Biomed 1997;10:394-410.
17. Hayes CE, Mathis CM, Yuan C. Surface coil phased arrays for high resolution imaging of the carotid arteries. Mag Res Imag 1996;6(1):109-112.
18. Liffers A, Quick HH, Herborn CU, Ermert H, Ladd ME. Geometrical optimization of a phased array coil for high-resolution MR imaging of the carotid arteries. MRM 2003;50(2):439-443.

19. Balu N, Yarnykh VL, Scholnick J, Chu B, Yuan C, Hayes C. Improvements in Carotid Plaque Imaging Using a New Eight-Element Phased Array Coil at 3T. Mag Res Imag 2009;30:1209-1214.
20. Kumar A, Edelstein WA, Bottomley PA. Noise Figure Limits for Circular Loop MR Coils. MRM (2009);61:1201-1209.
21. Roemer PB, Edelstein WA, Hayes CE, Souza SP, Mueller OM. The NMR Phased Array. MRM 1990;16:192-225.
22. Wiggins GC, Triantafyllou C, Potthast A, Reykowski A, Nittka, Wald LL. 32-Channel 3 Tesla Receive-Only Phased-Array Head Coil With Soccer-Ball Element Geometry. MRM 2006;56:216-223.
23. Griswold MA, Jakob PM, Heidemann RM, Nittka M, Jellus V, Wang J, Kiefer B, Haase A. Generalized Autocalibrating Partially Parallel Acquisitions (GRAPPA). MRM 2002;47:1202-1210.
24. Wiesinger F, Boesiger P, Pruessmann KP. Electrodynamics and Ultimate SNR in Parallel MR Imaging. MRM 2004;52:376-390.
25. Mendes J, Parker DL. Intrinsic detection of motion in segmented sequences. MRM 2010; Nov 3 (web published)

Figure 1. Head, neck and shoulders phantom. Custom fiberglass phantom filled with homogenous copper sulfate solution. This phantom was used for non-human rSNR comparisons.

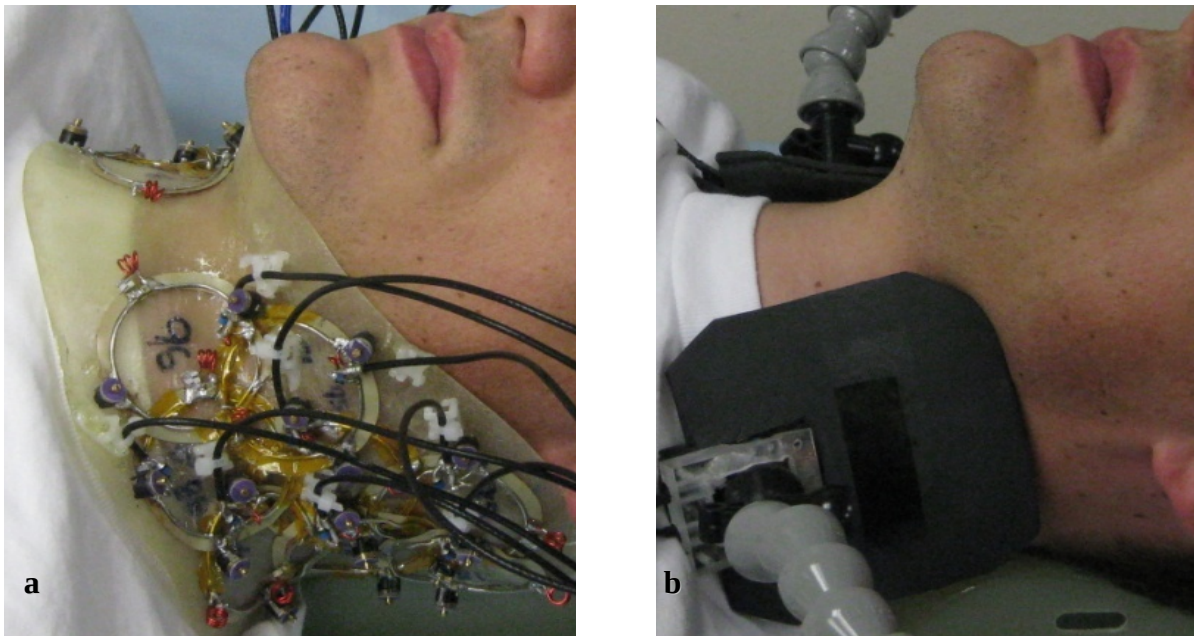

Figure 2. Placement of carotid coils used at our institution. **a)**16ch carotid coil on semi-rigid coil former assures a tight fitting coil and **b)** 4ch coil with flexible two paddle design.

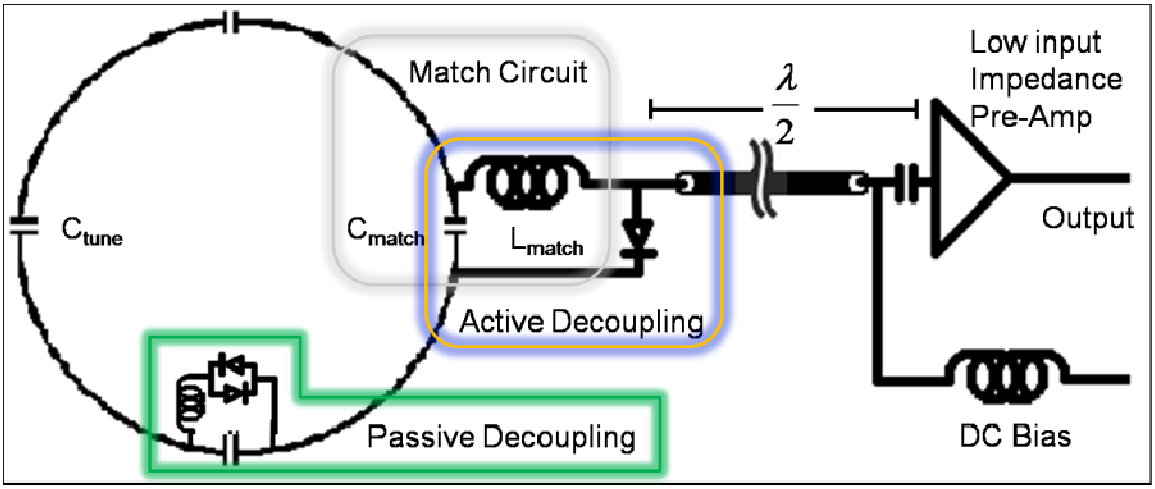

Figure 3. Schematic of the circuitry used for each individual coil element. This shows the match circuit as well as the passive and active decoupling and the pre-amp connection.

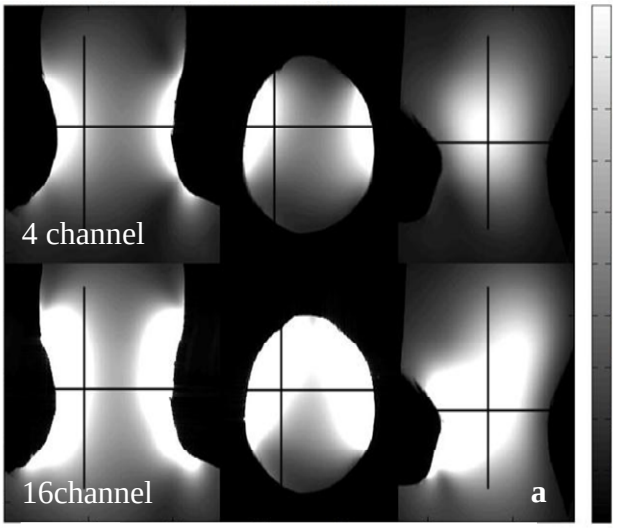

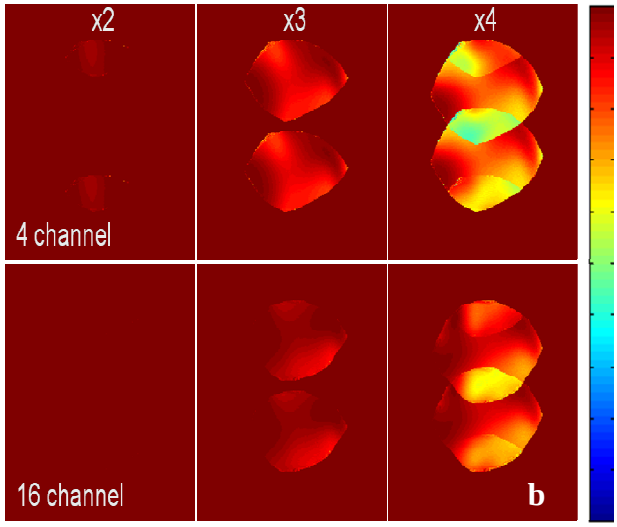

4. Phantom images and 1/g factor
) Coronal, Axial and Sagittal rSNR
of a phantom filled with a
nous copper sulfate solution. Slices
ɔnd to the average measured depth
erior/inferior position of the carotid
on in human scans used in this study.
ıctor maps (A/P) used to predict
l improvements in parallel imaging of
er 4ch.

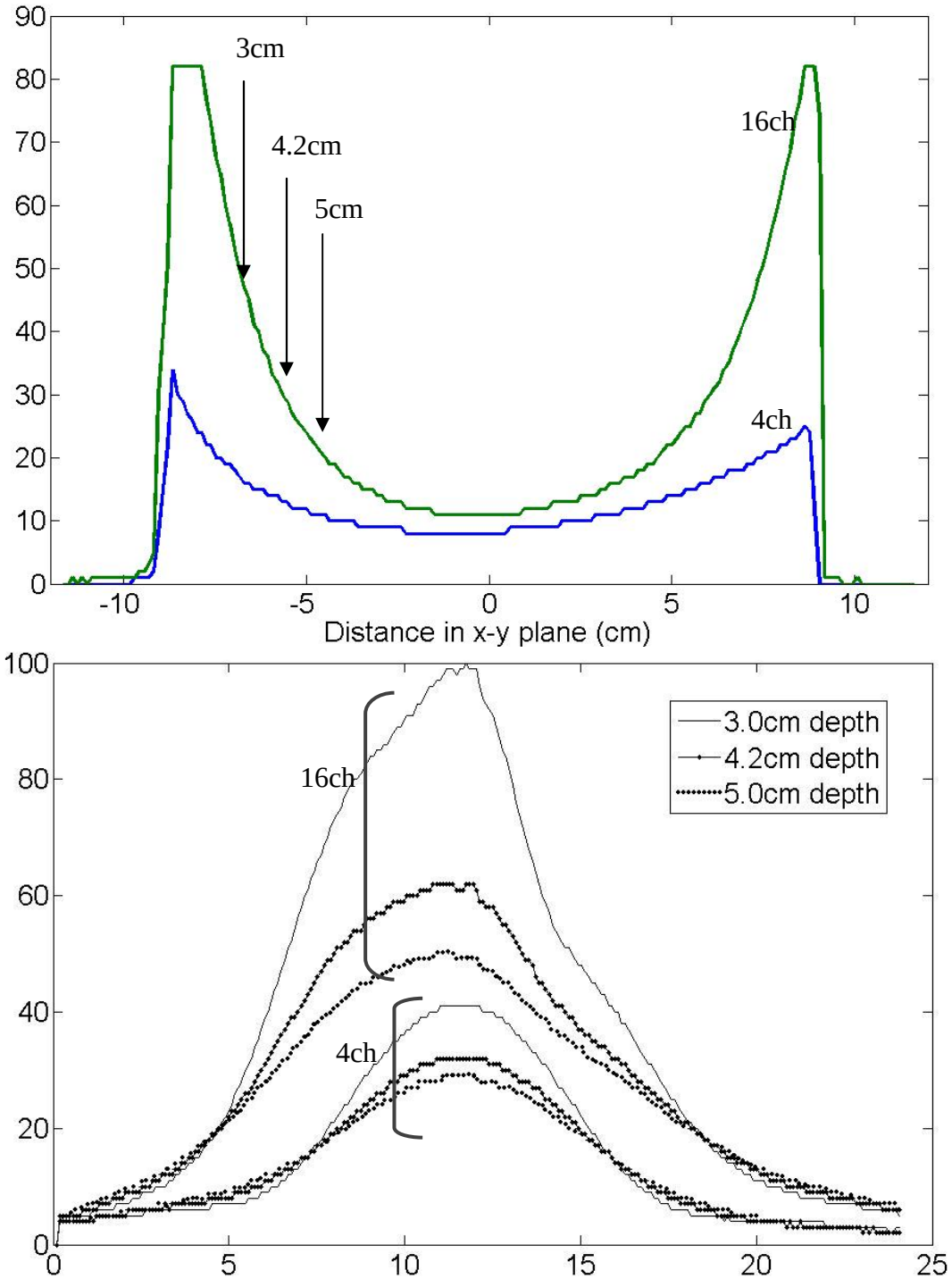

Figure 5. Line profile plots from phantom rSNR images. a) Transverse rSNR line profile of coronal slice at a depth (front/back) equal to the measured average of the carotid bifurcation. b) Sagittal rSNR line profile at depth (left/right) equal to the average measured depth of bifurcation.

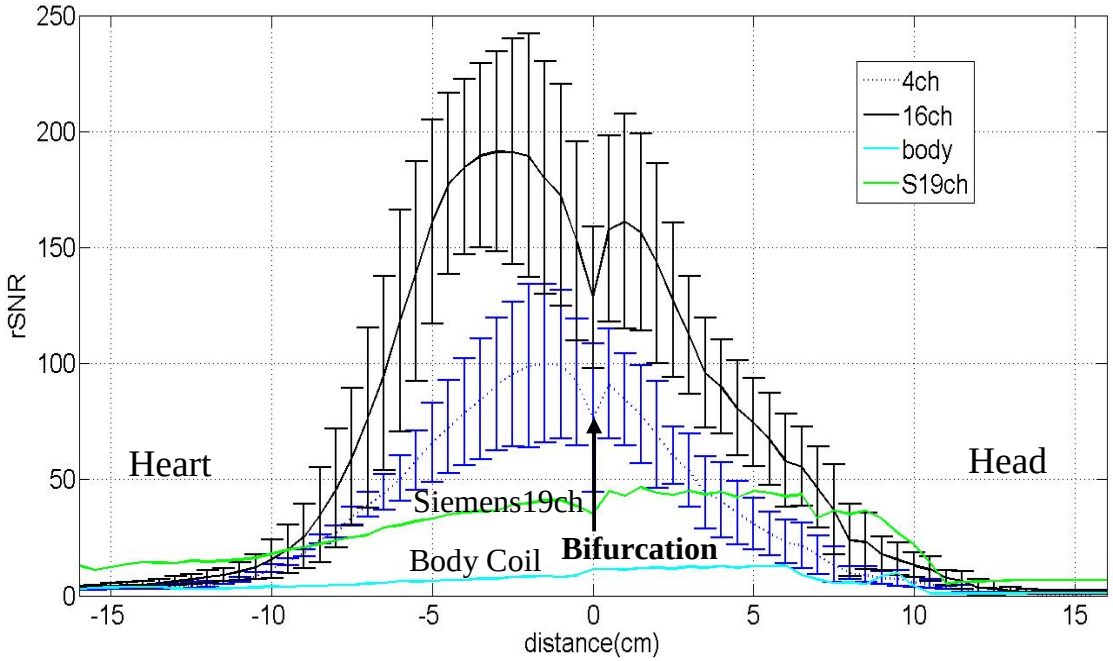

Figure 6. Profile plot of vessel axial rSNR traced from the circle of Willis to the aortic arch. Peak 4ch rSNR was normalized to 100 in order to simply show percent improvement of 16ch rSNR. Error bars show the standard deviation of rSNR for the group at each slice. Patient data were aligned and centered by the location of their bifurcation.

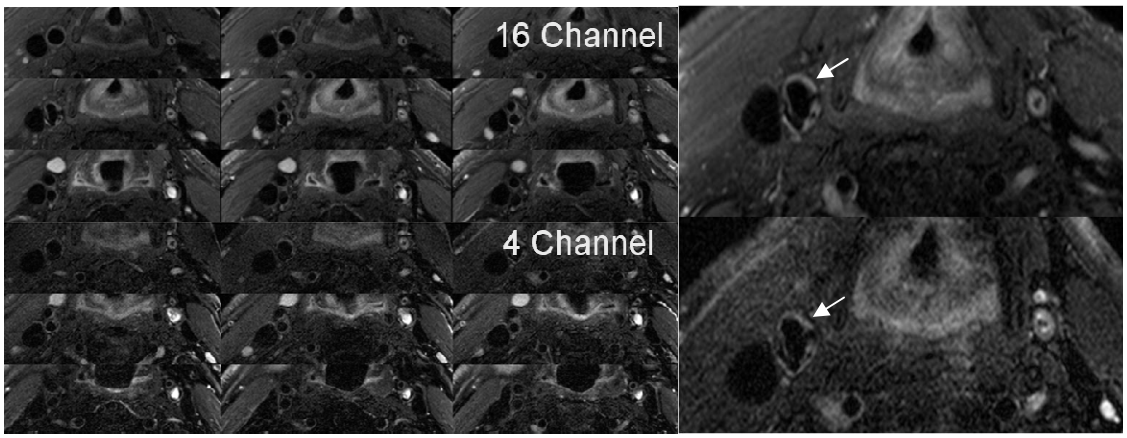

Figure 7. Clinical image demonstrating appearance of disease with different carotid coils using parallel imaging. Images were acquired with a 2D GRAPPA(R=2) T2 weighted TSE sequence. a) Image series showing comparison of 4ch and 16ch coils with a patient who has noticeable arterial disease. b)Enlarged images of the same series showing improvement in image clarity.

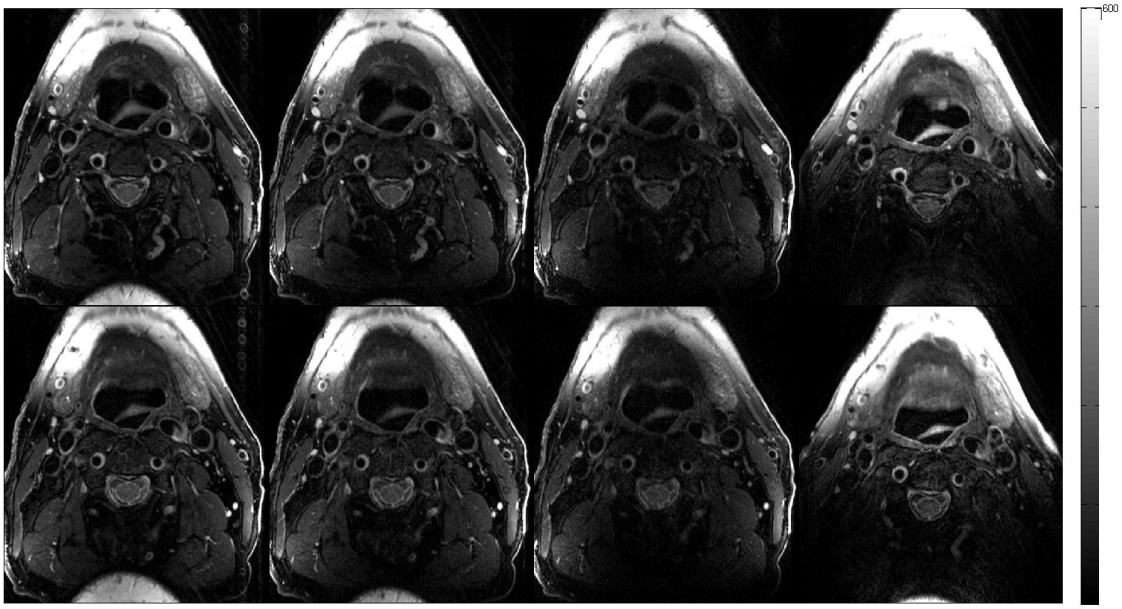

Figure 8. Clinical images further demonstrating improvements in parallel imaging. Images were acquired with a 2D GRAPPA (R=2) T2 weighted TSE sequence. The difference in image quality with the 16ch coil, using different reduction factors, compared to a R=2 using the 4ch coil is noticeable.

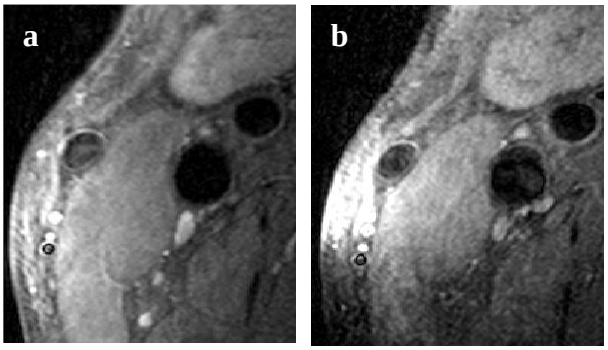

Figure 9. High resolution images (0.22x0.22 mm^2) comparing the a) 16ch and b) 4ch coils. The images show the improvement in definition with the 16ch as well as less artifact in both the internal and external carotid arteries.

CHAPTER 5

SUMMARY, CONCLUSIONS AND FUTURE WORK

5.1 Summary

MRI is a robust and powerful imaging modality that is non-invasive and does not use ionizing radiation. It has become an indispensible clinical tool. In order to fully utilize this tool it is essential to investigate the improvements that can be made with the hardware used in conjunction with the MRI scanner. A common thought to improve MRI image quality is to increase the strength of the magnetic field. This is expensive and not always a practical solution. Another way to improve the quality of the images is to improve the sensitivity of the coil used for imaging. An MRI coil is a specialized antenna array that is designed to function in the near field. There are a wide variety of implementations for these coils and many different types of specialized coil. My thesis research studied different methods for design and construction of a receive-only coil designed specifically to image the carotid arteries.

After considering several design options, including number and geometry of individual elements, a coil was designed and built for my undergraduate senior thesis work [2]. In continuation of this work, my thesis has been to improve this design by improving the sensitivity of this coil. This was done by replacing several of the elements and improving the overlap distance of adjacent coils in order to reduce magnetic

coupling. Once the coil was updated, studies were done to show the improvements in SNR and image quality between my carotid coil (16-channel), the current research standard carotid coil (four-channel), and a commercially available coil used for carotid imaging.

The results of these studies showed an average improvement over the standard four-channel coil of 100% increase in SNR within 4 cm of the carotid bifurcation (a key anatomical marker to begin searching for signs of atherosclerotic plaques). Also, using parallel imaging techniques, my 16-channel carotid coil was able to acquire signals that produced images comparable to those from the four-channel coil, but in nearly half the time. Due to the increased coil sensitivity, advantages were also shown in high definition images. By selecting a smaller voxel (differentiated individual volumes of signal source) size the received signal was still strong enough to produce useful images.

5.2 Conclusions

The 16-channel RF coil was able to produce higher quality images and made it possible to reduce the scan time by nearly half or produce higher definition images while maintaining adequate SNR. This has shown that my thesis research is of potential clinical benefit as well. Also, this work provides more evidence to support the idea that by improving the coil sensitivity SNR can be increased without the drastic costs of increasing the strength of the magnetic field. With an SNR improvement of 100% near the bifurcation, and a significant improvement in vessel depiction along the full length of the carotid arteries, the 16-channel coil has surpassed the four-channel research standard carotid coil in performance. The four-channel coil is more diverse because it was

constructed as two bilateral paddles, each consisting of two channels. The four-channel coil has the ability to be placed virtually anywhere on the body. The 16-channel coil, designed specifically for the neck, is built on a semi-rigid fiberglass former that keeps each coil element in nearly the same position relative to each other. In most cases this maintains coil proximity to the patient, and may or may not play a role in improved parallel imaging capabilities. In the end the 16-channel coil preformed well with a variety of neck sizes and consistently maintained improved SNR over other specialized and commercially available coils.

5.3 Future work

This thesis has shown that while there are many benefits of a specialized carotid coil with greater sensitivity and improved parallel imaging capabilities there is more work that can be done. For example, although this coil improved the quality of images from parallel imaging techniques, the coil could be better optimized for parallel imaging of the carotid artery, which might be a very important tool clinically. Also, while the design of this coil has been robust enough to acquire high quality images from a wide variety of body types and sizes, it may be beneficial to have several coil sizes in order to provide a closer fitting coil for a broader patient population. The composition of the coil, necessary circuitry housing and cables of the current design is cumbersome and often requires two people to place the coil on the patient. It is expected that future work will also simplify this mechanical design so that a single person could more easily manage it.

REFERENCES

[1] Bernstein MA, King KF , Zhou XJ. *Handbook of MRI Pulse Sequences*. San Diego: Elsevier Academic Press(2004). p. 96

[2] Tate Q. Design and Testing of a 16-Channel Coil Array for Improved Magnetic Resonance Imaging of the Carotid Artery. Senior Thesis, University of Utah, 2009

[3] Brewer RG, Hahn EL. Atomic Memory. Sci. Am. 1984; 251(6), 50-57

[4] Mitchell M D, Kundel H L, Axel L, Joseph P M. Agarose as a Tissue Equivalent Phantom Material for NMR Imaging. Mag Res Imag 1986;4(3):263-266

[5] Zeng GL. Medical Image Reconstruction: A Conceptual Tutorial. Springer Press (2009)

[6] Hadley JR, Roberts JA, Goodrich KC, Buswell HR, Parker DL. Relative RF Coil Performance in Carotid Imaging. Mag Res Imag 2005;23:629-639.

[7] Mathew S, Boskamp E, Hoppel B, Locke EH, Blawat L, Wasserman BA,Wright SM. Optimization of Carotid Coils. Proc. Intl Soc Mag Res Med. 2004; 11:1550

[8] Hayes CE, Mathis CM, Yuan C. Surface Coil Phased Arrays for High Resolution Imaging of the Carotid Arteries. Mag Res Imag 1996;6(1):109-112.

[9] Balu N, Yarnykh VL, Scholnick J, Chu B, Yuan C, Hayes C. Improvements in Carotid Plaque Imaging Using a New Eight-Element Phased Array Coil at 3T. Mag Res Imag 2009;30:1209-1214.

[10] Liffers A, Quick HH, Herborn CU, Ermert H, Ladd ME. Geometrical Optimization of a Phased Array Coil for High-Resolution MR Imaging of the Carotid Arteries. MRM 2003;50(2):439-443.

[11] Merrill R, Parker D, Minalga E, Bell L, Rose J, Hadley R. Improved Optic Nerve Imaging Using a Collapsible Head Coil Design. Electronic-Poster Proc Intl Soc Mag Res Med 2009; 3851

[12] Tate Q, Bell LC, Kim SE, Minalga E, Parker DL, Hadley JR. A 16 Channel Radio Frequency Anterior Neck Coil for Imaging of the Cervical Carotid Bifurcation. Electronic-Poster Proc Intl Soc Mag Res Med. 2009; 3841

[13] Kumar A, Edelstein WA, Bottomley PA. Noise Figure Limits for Circular Loop MR Coils. MRM (2009);61:1201-1209.

[14] Roemer PB, Edelstein WA, Hayes CE, Souza SP, Mueller OM. The NMR Phased Array. MRM 1990;16:192-225.

[15] Wright SM, Wald LL. Theory and Application of Array Coils in MR Spectroscopy. NMR Biomed 1997;10:394-410.

[16] Wang Y. Description of Parallel Imaging in MRI Using Multiple Coils. Mag Res Med 2000;44:495-499.

[17] Redpath TW. Commentary: Signal-to-Noise Ratio in MRI. The British Journal of Radiology 1998; 71:704-707.